Scaled Boundary Finite Element Analysis of three-dimensional crack

configurations in laminate structures

†Sascha Hell¹, *Wilfried Becker¹

¹Department of Structural Mechanics, TU Darmstadt, Germany

*Presenting author: becker@fsm-tu-darmstadt.de †Corresponding author: hell@fsm-tu-darmstadt.de

Abstract

Laminate structures composed of fibre-reinforced plies typically are prone to the formation of interfiber cracks because of the given strongly anisotropic stiffness and strength properties. These interfiber cracks commonly run through complete plies but are stopped at the ply interfaces. Equally, such laminate structures are prone to the formation of delaminations, e.g. due to the free-edge effect. An inter-fiber crack meeting a delamination forms a non-standard three-dimensional crack configuration with a locally singular stress field that should be investigated in regard of its criticality.

For that purpose, the Scaled Boundary Finite Element Method turns out to be an appropriate and effective analysis method that permits solving linear elastic mechanical problems including stress singularities with comparably little effort. Only the boundary is discretized by two-dimensional finite elements while the problem is considered analytically in the direction of the dimensionless radial coordinate ξ . A corresponding separation of variables representation for the displacement field employed in the virtual work equation leads to a system of differential equations of Cauchy-Euler type. This differential equation system can be converted into an eigenvalue problem and solved by standard eigenvalue solvers for non-symmetric matrices.

By this kind of analysis, it is revealed that the considered three-dimensional crack configurations may go along with various unexpected non-standard stress singularities, namely singularities that are weaker than the well-known square root stress singularity in linear elastic fracture mechanics, but also singularities that are stronger and which may be called hypersingularities.

Keywords: Scaled Boundary Finite Element Method, laminate, inter-fiber crack, delamination, stress singularity

Introduction

Unidirectionally fiber-reinforced materials as they are used in structural components, exhibit a strongly anisotropic material behavior. They offer very high stiffness and strength properties in the fiber direction but low values in the transverse directions. This makes them prone to the formation of matrix cracks between the fibers, so-called inter-fiber cracks. In a laminated structure of unidirectionally fiber-reinforced plies, these inter-fiber cracks, at first, only lead to some stiffness degradation but also to locally new structural situations with a highly complex failure evolution (see e.g. [Leguillon and Martin (2012)]). Because of this complexity and moreover the lack of predictability of the failure evolution, it is still common practice in industrial composite design to assume laminate failure when the so-called First-Ply-Failure occurs, i.e. when the first inter-fiber cracks emerge. Especially for quasi-isotropic carbon fiber reinforced plastic (CFRP) laminates with a ply lay-up of the kind [±45°/0°/90°]s as they are almost exclusively used in the aircraft industry, this assumption dramatically underestimates the true load bearing capacity of such a composite laminate. To achieve further progress in this field, it is crucial to gain a proper understanding of these structural situations and their possible interactions with other defects. Such other defects are e.g. delaminations which commonly occur due to impact loads or also as a consequence of the laminate free-edge effect. A delamination meeting a transverse inter-fiber crack is, thus, a possible crack configuration that needs closer investigation.

A special challenge of such structural situations within the framework of linear elasticity theory is the occurrence of theoretically infinite stresses. Stress singularities typically occur at discontinuities of geometry and material. The near-field solution at a singular point for the displacements and stresses respectively is usually represented by a power law function series of the kind

$$\vec{u}(r,\varphi,\theta) = \sum_{j=1}^{\infty} c_{uj} r^{\lambda_j} (\ln r)^k \vec{\Phi}_{uj}(\varphi,\theta) \quad , \quad \mathbf{\sigma}(r,\varphi,\theta) = \sum_{j=1}^{\infty} c_{\sigma_j} r^{\lambda_j-1} (\ln r)^k \mathbf{\Phi}_{\sigma_j}(\varphi,\theta)$$
(1)

given in spherical coordinates r, φ, ϑ . Here, λ_j are complex numbers and $\bar{\Phi}_{uj}$ and $\Phi_{\sigma j}$ are vector and tensor functions of the angle coordinates φ and ϑ . For $\text{Re}(\lambda_j)-1<0$ and $r\to 0$ the stress tensor becomes singular and the quantities $\text{Re}(\lambda_j)-1$ are called stress singularity exponents. The free constants c_{uj} and $c_{\sigma j}$ are not independent of each other and need to be determined from the boundary conditions. However, this means that it depends on the boundary conditions whether a stress singularity actually occurs. The exponent k depends on the geometrical multiplicity of λ_j and is zero in most cases.

Stress singularities can be classified into weak and strong singularities between which the classical crack singularity of $Re(\lambda_j)-1=-0.5$ constitutes the threshold value. [Leguillon and Sanchez-Palencia (1999)] showed that for 2D as well as 3D situations, weak singularities yield a differential energy release rate of $\mathcal{G}=0$. This means that crack configurations evolving towards a structural situation with a weak stress singularity tend to a crack arrest. This, for example, is the case for a crack under mode I loading growing perpendicularly towards an interface with a stiffer material (e.g. [Leguillon and Martin (2012; 2013)]). On the contrary, strong singularities, which also may be called hypersingularities, are characterized by a differential energy release rate which tends to infinity $\mathcal{G} \to \infty$. This means that structural situations under a loading producing a hypersingularity, but also neighboring crack configurations evolving towards such a structural situation, tend to a further, instable crack growth. This, for example, is the case for a crack under mode I loading growing perpendicularly towards an interface with a less stiff material. In conclusion, weak singularities can be classified as less critical and hypersingularities as more critical than the classical crack singularity.

An appropriate method for linear elastostatic problems, which is capable of both resolving the singularities in 3D structural situations and taking into account different anisotropic materials and interfaces, is the Scaled Boundary Finite Element Method (SBFEM). Its suitability for 2D problems has been demonstrated e.g. by [Song (2006)] and for 3D problems e.g. by [Mittelstedt and Becker (2005)] and [Goswami and Becker (2012)]. In a former work, the SBFEM has furthermore been successfully used by [Hell and Becker (2014)] for the analysis of two meeting transverse inter-fiber cracks in a composite laminate. A very similar method based on an FEM eigenanalysis has also proven to be adequate: [Bažant and Estenssoro (1979)], [Somaratna and Ting (1986)], [Gharemani (1991)], [Dimitrov et al. (2001)], [Koguchi and da Costa (2010)], [Korepanova et al. (2013)] are only a few authors who employed that method.

In the following, a brief description of the SBFEM is given before it will be employed for the analysis of a delamination meeting a transverse inter-fiber crack.

The Scaled Boundary Finite Element Method

The Scaled Boundary Finite Element Method (SBFEM) ([Deeks and Wolf (2002)], [Song and Wolf (1997)], [Wolf (2003)] is a semi-analytical method which combines the advantages of the Boundary Element Method (BEM) and the Finite Element Method (FEM). Comparable to the BEM, only the boundary, or in some cases even only parts of the boundary, need to be discretized. At the same time, the problem of strongly singular integrands, present in the BEM-approach, does not exist in the SBFEM. This is because the SBFEM is based on a variational principle and does not need any fundamental solutions. As a further consequence of this, arbitrary linear elastic material behavior in three dimensions can be taken into account in a Scaled Boundary Finite Element. This makes the SBFEM a powerful tool for a variety of linear elasticity problems, which has lately also been extended to nonlinear analyses (e.g. [Behnke et al. (2014), Ooi et al. (2014)]).

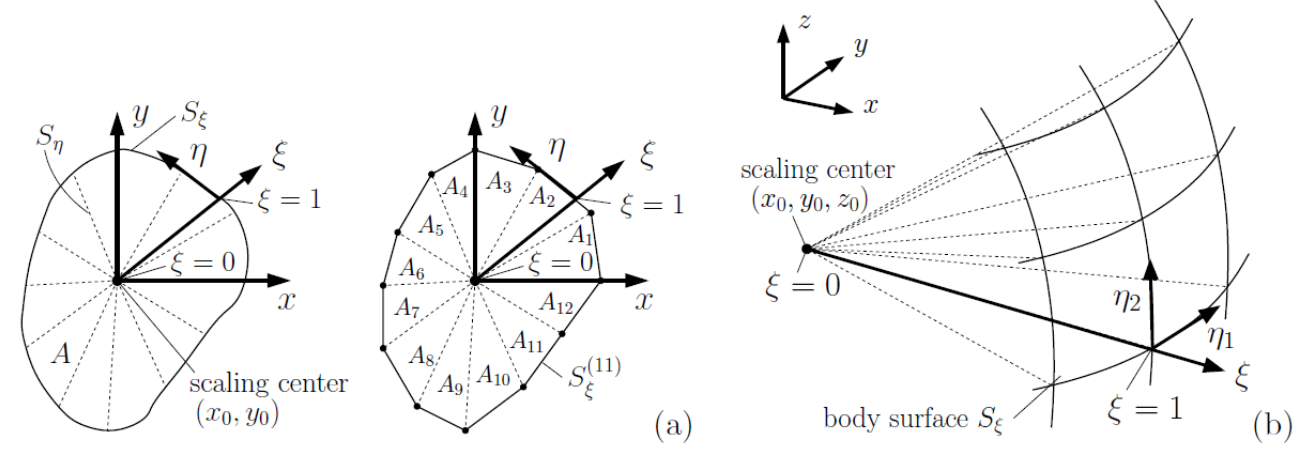


Figure 1: Scaled Boundary Coordinate System and discretization scheme in a (a) 2D and a (b) 3D example.

The *geometrical scalability* is a fundamental requirement of the SBFEM. It requires that the connection of any point on the boundary with the scaling center by a straight line must be possible without any further intersections. Accordingly, a scaled boundary coordinate system is defined having its origin at the scaling center with the coordinates (x_0, y_0, z_0) in a Cartesian coordinate system. The scaling coordinate ξ runs from the scaling center $\xi = 0$ to the boundary $\xi = 1$. In case of a 2D problem, a boundary coordinate η runs along the boundary. In case of a 3D problem, two boundary coordinates η_1 and η_2 describe the surface of the body. Figure 1 illustrates this procedure for the example of an arbitrarily shaped 2D domain and how it can be extended to 3D domains. The Cartesian coordinates are expressed in terms of the scaled boundary coordinates:

$$x = x_0 + \xi \cdot x_\eta(\eta_1, \eta_2) \quad , \quad y = y_0 + \xi \cdot y_\eta(\eta_1, \eta_2) \quad , \quad z = z_0 + \xi \cdot z_\eta(\eta_1, \eta_2). \tag{2}$$

The partial differential operators are calculated by the use of the Jacobian matrix **J**:

$$\begin{bmatrix}
\frac{\partial}{\partial \xi} \\
\frac{\partial}{\partial \eta_{1}} \\
\frac{\partial}{\partial \eta_{2}}
\end{bmatrix} = \begin{bmatrix}
\frac{\partial \mathbf{x}}{\partial \xi} & \frac{\partial \mathbf{y}}{\partial \xi} & \frac{\partial \mathbf{z}}{\partial \xi} \\
\frac{\partial \mathbf{x}}{\partial \lambda} & \frac{\partial \mathbf{y}}{\partial y} & \frac{\partial \mathbf{z}}{\partial z} \\
\frac{\partial \mathbf{z}}{\partial \lambda} & \frac{\partial \mathbf{y}}{\partial y} & \frac{\partial \mathbf{z}}{\partial z}
\end{bmatrix} \begin{bmatrix}
\frac{\partial}{\partial \mathbf{x}} \\
\frac{\partial}{\partial y} \\
\frac{\partial}{\partial z}
\end{bmatrix} = \begin{bmatrix}
\mathbf{x}_{\eta} & \mathbf{y}_{\eta} & \mathbf{z}_{\eta} \\
\mathbf{x}_{\eta,\eta_{1}} & \mathbf{y}_{\eta,\eta_{2}} & \mathbf{z}_{\eta,\eta_{1}} \\
\mathbf{x}_{\eta,\eta_{2}} & \mathbf{y}_{\eta,\eta_{2}} & \mathbf{z}_{\eta,\eta_{2}}
\end{bmatrix} \begin{bmatrix}
\frac{\partial}{\partial \mathbf{x}} \\
\frac{\partial}{\partial y} \\
\frac{\partial}{\partial z}
\end{bmatrix} = \mathbf{J} \begin{bmatrix}
\frac{\partial}{\partial \mathbf{x}} \\
\frac{\partial}{\partial y} \\
\frac{\partial}{\partial z}
\end{bmatrix}.$$
(3)

The notation $(\cdot)_{,\eta}$ is to be read as the partial derivative $\partial(\cdot)/\partial\eta_1$. Please note that in this notation the Jacobian $\mathbf{J}(\eta_1,\eta_2)$ is only a function of the boundary coordinates so that the volumetric differential can be written as

$$dV = || \mathbf{J}(\eta_1, \eta_2) || \xi^2 d\xi d\eta_1 d\eta_2. \tag{4}$$

A separation of variables ansatz is made for the displacements and separates dependences of the boundary coordinates η_1, η_2 from dependences of the scaling coordinate ξ . However, the resulting equations still cannot be solved analytically so that an approximative approach is needed. Only the boundaries S_{ξ} where $\xi = \text{const}$, are discretized using isoparametric finite elements and shape functions $N_j(\eta_1,\eta_2)$. This sub-divides the body into a number of wedge-shaped domains which are denoted Scaled Boundary Finite Elements (Figure 1). The problem is still considered analytically in the scaling coordinate ξ . Thus, vector functions $\vec{u}_j^{(e)}(\xi)$ are introduced for the displacements on rays pointing from the scaling center to the finite element nodes on the boundary. The superscript $(\cdot)^{(e)}$

denotes the formulation within a Scaled Boundary Finite Element e where the shape functions are combined to the matrix $\mathbf{N}(\eta_1, \eta_2)$ and the vector functions $\vec{u}_j^{(e)}(\xi)$ to $\vec{U}^{(e)}(\xi)$ \$. A similar approximative approach is chosen for the virtual displacements:

$$\tilde{\vec{u}}^{(e)}(\xi,\eta_1,\eta_2) = \mathbf{N}(\eta_1,\eta_2) \, \vec{U}^{(e)}(\xi) \qquad , \qquad \delta \tilde{\vec{u}}^{(e)}(\xi,\eta_1,\eta_2) = \mathbf{N}(\eta_1,\eta_2) \, \delta \vec{U}^{(e)}(\xi). \tag{5}$$

Like the FEM, the SBFEM is based on the principle of virtual work

$$\delta W_i = \int_V \mathbf{\sigma} : \delta \mathbf{\epsilon} dV = \int_V \vec{f} \cdot \delta \vec{u} dV + \int_{S_i} \vec{t} \cdot \delta \vec{u} dA = \delta W_a$$
 (6)

where σ , $\delta \varepsilon$, \vec{t} , $\delta \vec{u}$, \vec{t} are the stress tensor, the virtual strain tensor, body forces, virtual displacements and prescribed boundary tractions respectively. δW_i is the internal and δW_a the external virtual work. V is the volume of the considered domain and S_t the part of the domain surface with prescribed traction boundary conditions.

We use the vector notation for stresses and strains and introduce a differential operator L

$$\mathbf{L}^{T} = \begin{bmatrix} \frac{\partial}{\partial x} & 0 & 0 & 0 & \frac{\partial}{\partial z} & \frac{\partial}{\partial y} \\ 0 & \frac{\partial}{\partial y} & 0 & \frac{\partial}{\partial z} & 0 & \frac{\partial}{\partial x} \\ 0 & 0 & \frac{\partial}{\partial z} & \frac{\partial}{\partial y} & \frac{\partial}{\partial x} & 0 \end{bmatrix}$$
(7)

which is used in the equilibrium equations and strain-displacement relations. This differential operator L is then transformed into scaled boundary coordinates. To this end, L is decomposed into three matrices L_x, L_y, L_z each associated to one partial differential operator in the Cartesian coordinate system. Then, each partial differential operator can be replaced by its respective counterpart in the scaled boundary coordinate system which yields

$$\mathbf{L} = \mathbf{L}_{x} \frac{\partial}{\partial x} + \mathbf{L}_{y} \frac{\partial}{\partial y} + \mathbf{L}_{z} \frac{\partial}{\partial z} = \mathbf{b}_{\xi} \frac{\partial}{\partial \xi} + \mathbf{b}_{\eta_{1}} \frac{1}{\xi} \frac{\partial}{\partial \eta_{1}} + \mathbf{b}_{\eta_{2}} \frac{1}{\xi} \frac{\partial}{\partial \eta_{2}}.$$
 (8)

Employment of the differential operator L(7) and the separation of variables ansatz (5) in the strain-displacement relations in vector notation yields:

$$[\varepsilon] = \mathbf{L} \, \mathbf{N}(\eta_1, \eta_2) \, \vec{U}(\xi) = \underbrace{\mathbf{b}_{\xi} \, \mathbf{N}}_{\mathbf{B}_{\xi}(\eta_1, \eta_2)} \frac{\partial \vec{U}(\xi)}{\partial \xi} + \underbrace{\left[\mathbf{b}_{\eta_1} \, \mathbf{N}_{,\eta_1} + \mathbf{b}_{\eta_2} \, \mathbf{N}_{,\eta_2}\right]}_{\mathbf{B}_{\eta}(\eta_1, \eta_2)} \vec{\xi}. \tag{9}$$

Additionally, Hooke's law $[\sigma] = \mathbf{C}[\varepsilon]$ (linear elastic material behavior) with the elasticity matrix \mathbf{C} is used in the virtual work balance (6). Assuming that the relations for the real quantities are also valid for the virtual ones leads to the virtual work balance in terms of the displacements and virtual displacements in scaled boundary coordinates.

$$\int_{V} \left[\delta \vec{U}_{,\xi}^{T} \mathbf{B}_{\xi}^{T} + \delta \vec{U}^{T} \mathbf{B}_{\eta}^{T} \frac{1}{\xi} \right] \mathbf{C} \left[\mathbf{B}_{\xi} \vec{U}_{,\xi} + \mathbf{B}_{\eta} \vec{U} \frac{1}{\xi} \right] dV \stackrel{!}{=} \int_{V} \delta \vec{U}^{T} \mathbf{N}^{T} \vec{f} dV + \int_{S_{t}} \delta \vec{U}^{T} \mathbf{N}^{T} \vec{t}^{*} dA$$

$$(10)$$

Expansion of the product and integration by parts over ξ in the internal virtual work term δW_i yields an arithmetic expression containing factors which are either dependent of the scaling variable ξ or of the boundary coordinates η_1, η_2 . Hence, the integration can be performed separately. The dependence of η_1 and η_2 actually is one of the introduced shape functions $\mathbf{N}(\eta_1, \eta_2)$ so that numerical integration over the boundary coordinates can be used. This yields the following matrices within one Scaled Boundary Finite Element e:

$$\mathbf{E}_{0}^{(e)} = \int_{\mathbf{S}_{\xi}^{(e)}} \mathbf{B}_{\xi}^{T}(\eta_{1}, \eta_{2}) \mathbf{C} \, \mathbf{B}_{\xi}(\eta_{1}, \eta_{2}) \| \, \mathbf{J}^{(e)}(\eta_{1}, \eta_{2}) \| \, \mathrm{d}\eta_{1} \, \mathrm{d}\eta_{2},
\mathbf{E}_{1}^{(e)} = \int_{\mathbf{S}_{\xi}^{(e)}} \mathbf{B}_{\eta}^{T}(\eta_{1}, \eta_{2}) \mathbf{C} \, \mathbf{B}_{\xi}(\eta_{1}, \eta_{2}) \| \, \mathbf{J}^{(e)}(\eta_{1}, \eta_{2}) \| \, \mathrm{d}\eta_{1} \, \mathrm{d}\eta_{2},
\mathbf{E}_{2}^{(e)} = \int_{\mathbf{S}_{\xi}^{(e)}} \mathbf{B}_{\eta}^{T}(\eta_{1}, \eta_{2}) \mathbf{C} \, \mathbf{B}_{\eta}(\eta_{1}, \eta_{2}) \| \, \mathbf{J}^{(e)}(\eta_{1}, \eta_{2}) \| \, \mathrm{d}\eta_{1} \, \mathrm{d}\eta_{2}.$$
(11)

In numerical integration, attention must be paid to the Jacobian determinant when the discretized body surface is curved. Then, the numerical integration error needs to be monitored.

The matrices $\mathsf{E}_0^{(e)}, \mathsf{E}_1^{(e)}, \mathsf{E}_2^{(e)}$ are similarly assembled like in the standard Finite Element Method. This yields the following form of the virtual work balance for the case of a 3D bounded domain $\xi = 0...1$:

$$\delta W_{i} = -\int_{\xi=0}^{1} \delta \vec{U}^{T}(\xi) \Big[\mathbf{E}_{0} \xi^{2} \vec{U}(\xi)_{,\xi\xi} + \left[2\mathbf{E}_{0} + \mathbf{E}_{1}^{T} - \mathbf{E}_{1} \right] \xi \vec{U}(\xi)_{,\xi} + \left[\mathbf{E}_{1}^{T} - \mathbf{E}_{2} \right] \vec{U}(\xi) \Big] d\xi + \delta \vec{U}^{T}(\xi) \Big[\mathbf{E}_{0} \xi^{2} \vec{U}(\xi)_{,\xi} + \xi \mathbf{E}_{1}^{T} \vec{U}(\xi) \Big]_{\xi=0}^{1} \stackrel{!}{=} \delta W_{a}.$$

$$(12)$$

This equation contains one integral term and two boundary terms ($\xi = 0,1$). The boundary terms represent the forces which the continuum exerts on the boundary S_{ξ} . Assuming the absence of side face loads, i.e. tractions at the side faces S_{η} where either η_1 or η_2 are constant, and that body forces are negligible, the virtual external work can be reduced to $\delta W_a = \delta \bar{U}^T(1) \, \bar{p}_{\xi=1}$. The assembled nodal loads vector $\bar{p}_{\xi=1}$ gives a contribution to the boundary term in eq. (12). The resulting virtual work balance is valid for arbitrary virtual displacements if and only if the integrand in eq. (12) and the boundary terms are zero each. This yields a homogeneous system of differential equations of Cauchy-Euler type and a linear equation system. A solution fulfilling the homogeneous differential equation system is only approximated over the body surface but analytic in ξ . The system of linear equations serves for enforcing the boundary conditions on the discretized body surface S_{ξ} .

Solution of the homogeneous differential equation system

By application of a variable transformation $t = \ln \xi$, a differential equation system of Cauchy-Euler type can be transformed into an ordinary one with constant coefficients. The introduction of the vector function $\vec{V}(t) = \vec{U}(t)$, then allows the further transformation of the differential equation system of second order into one of first order but at the cost of doubling the number of degrees of freedom.

$$\underbrace{\begin{bmatrix} \vec{V}(t)_{,t} \\ \vec{U}(t)_{,t} \end{bmatrix}}_{\vec{W}(t)_{,t}} = \underbrace{\begin{bmatrix} -\mathbf{E}_{0}^{-1} \begin{bmatrix} \mathbf{E}_{1}^{T} - \mathbf{E}_{1} \end{bmatrix} - \mathbf{I} & -\mathbf{E}_{0}^{-1} \begin{bmatrix} \mathbf{E}_{1}^{T} - \mathbf{E}_{2} \end{bmatrix}}_{\mathbf{K}} \underbrace{\begin{bmatrix} \vec{V}(t) \\ \vec{U}(t) \end{bmatrix}}_{\vec{W}(t)} \tag{13}$$

The fundamental solution solving this type of differential equations converts the differential equation system into an eigenvalue problem.

$$\vec{W}_j(t) = \vec{\Phi}_j \, e^{\lambda_j t} \quad \Rightarrow \quad \lambda_j \, \vec{\Phi}_j = \mathbf{K} \, \vec{\Phi}_j \tag{14}$$

By application of established numerical algorithms, even non-symmetric and rather large eigenvalue problems can be solved. Unfortunately, these algorithms suffer from numerical errors, which are not negligible any more if the magnitudes of neighboring eigenvalues move closer together. Nevertheless, small eigenvalues close to zero and associated eigenvectors generally are of good quality and converge appropriately with a discretization refinement.

The backtransformation of the fundamental solution $(t \to \xi : \vec{W}_j(\xi) = \vec{\Phi}_j \xi^{\lambda_j})$ reveals that the eigenvectors can be interpreted as deformation modes and that the eigenvalues are their associated decay $(\text{Re}(\lambda_j) < 0)$ or growth rates $(\text{Re}(\lambda_j) > 0)$. In fact, only the lower half of the eigenvector $\vec{\Phi}_{uj}$ represents a deformation mode while the upper half is simply given by $\vec{\Phi}_{vj} = \vec{\Phi}_{uj}\lambda_j$. The eigenvalue spectrum in the 3D case is symmetric to -0.5, which also marks the value of a bounded domain for which the strain energy density tends to infinity. Complex eigenvalues always appear as conjugate pairs $\lambda = \alpha \pm i\beta$. In the case of geometric multiplicity, i.e. for a given number of equal eigenvalues, not the same number of linearly independent eigenvectors exists, additional generalized eigenvectors have to be generated resulting in logarithmic deformation modes to complete the solution. Hence, the general solution of the differential equation system with N different eigenpairs of geometric multiplicity n_j is

$$\vec{W}(\xi) = \sum_{j=1}^{N} \sum_{k=0}^{n_j-1} \left[\text{Re}\left(\vec{\Phi}_{jk} e^{i\beta_j \ln \xi}\right) c_{jk1} + \text{Im}\left(\vec{\Phi}_{jk} e^{i\beta_j \ln \xi}\right) c_{jk2} \right] \xi^{\alpha_j} (\ln \xi)^k. \tag{15}$$

Here, c_{jk1} and c_{jk2} are free constants. In sum, they are of the number of twice the number of degrees of freedom of the approximated boundary value problem. These free constants are determined from regularity and boundary conditions.

Delamination Meeting a Transverse Inter-Fiber Crack in a Composite Laminate

The 3D structural situation of a delamination meeting a transverse inter-fiber crack which runs through the complete ply can more generally be described as two plane cracks with straight crack fronts meeting each other at an interface. But in contrast to the structural situation studied in [Hell and Becker (2014)], where the mode I crack growth directions of the two cracks point towards each other representing the situation of two meeting transverse inter-fiber cracks, the mode I crack growth directions here are assumed to be perpendicular to each other. This also implies that the transverse inter-fiber crack can, in a way, be seen as dividing the delamination crack in two parts. Configurations with angles between the crack fronts $15^{\circ} < 9 < 90^{\circ}$ and concurrent ply lay-ups $[(90^{\circ} - 9)/90^{\circ}]$ are considered (cf. Figure 2). The stress singularity exponents $Re(\lambda_{j}) - 1$ and their associated deformation modes $\bar{\Phi}_{uj}(\eta_{1},\eta_{2})$ are calculated by means of the SBFEM using a spherical boundary mesh for a minimum numerical effort. Between 931 and 1406 bilinear isoparametric SBFEs for the angles $9 = 60^{\circ}$ and $9 = 35^{\circ}$, respectively, are used for the boundary mesh, which is in each case appropriately refined at the crack fronts. The results for the absolute values of the stress singularity exponents $1 - Re(\lambda_{j})$ are presented in Figure 3 and Figure 4.

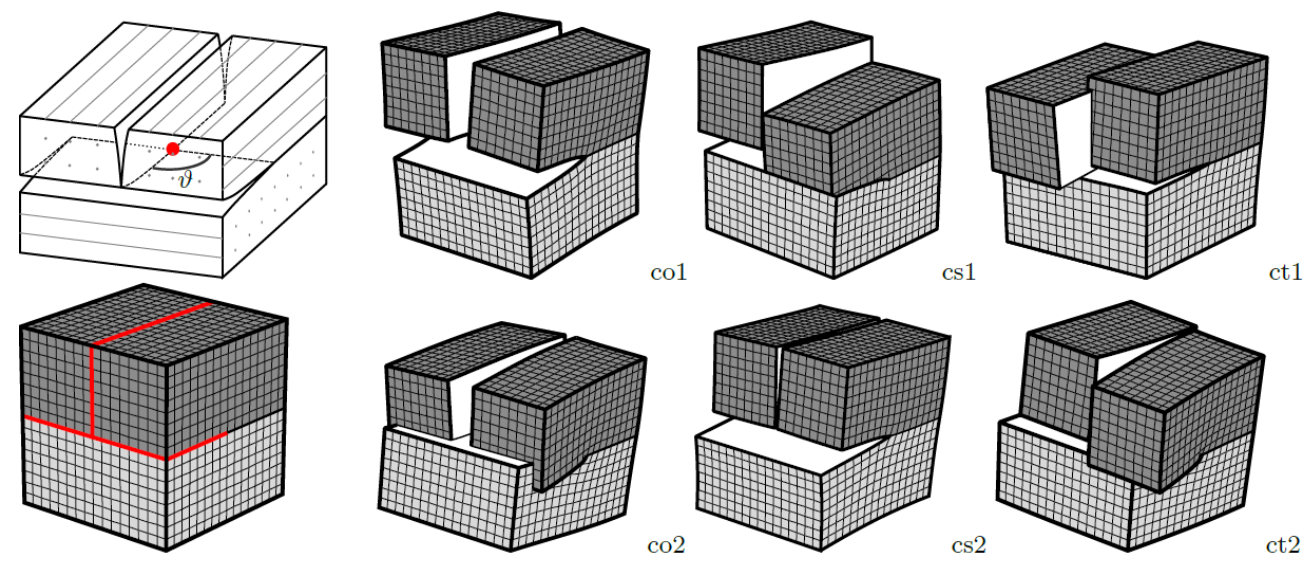


Figure 2: Delamination crack meeting transverse inter-fiber crack in a fiber-reinforced composite laminate with angle ϑ between the crack fronts and used boundary mesh. 6 singular deformation modes for $\vartheta=90^\circ$: crack opening (co1/2), shearing (cs1/2) and twisting (ct1/2).

Figure 3 gives the results for a T800/epoxy (a carbon fiber reinforced plastic) laminate revealing 6 stress singularities. The 6 associated deformation modes are shown in Figure 2 for the example of $\theta = 90^{\circ}$. For an easier identification, they are presented for a cubic boundary mesh where the cracks implemented as double nodes are marked in red. The upper half (dark shading) represents the upper ply with a 0°-orientation and contains the correspondingly aligned transverse inter-fiber crack. The lower half (light shading) represents the lower ply with 90°-orientation. The delamination crack is located at the interface, which obviously coincides with the plane defined by the present crack fronts. The deformation mode col corresponds to a simultaneous crack opening of the delamination and the inter-fiber crack. On the other hand, deformation mode co2 corresponds to a crack opening of only one of the cracks and a crack closing of the other. The deformation mode cs1 corresponds to a crack shearing of the inter-fiber crack, which implies a simultaneous crack opening respectively closing of the delamination crack faces. A crack shearing of the delamination crack can be identified for deformation mode cs2. The deformation mode ct1 corresponds to a crack twisting of the inter-fiber crack, which implies a simultaneous counter-directional crack shearing of the delamination crack. A kind of crack twisting of the delamination crack can be identified for the deformation mode ct2. Although these deformation modes actually only correspond to the particular case of $\theta = 90^{\circ}$, the wording is kept for all configurations studied. Other crack configurations with different angles 9 between the crack fronts produce different deformation modes for which the individual crack deformations cannot be assigned equally clearly to the classical single-crack deformation modes any more. Please note that deformation mode cs2 is an exception and constitutes the only deformation mode remaining widely unchanged for all configurations presented in this work. At the same time, cs2 is the deformation mode most closely related to a pure singlecrack deformation mode, namely mode II of the delamination crack. This makes, indeed, perfectly sense as a corresponding mode II delamination crack loading does not require an exchange of forces through the inter-fiber crack faces. In fact, its corresponding stress singularity exponent remains close to the classical crack singularity exponent of $1-Re(\lambda)=0.5$ for all angles θ and material combinations considered.

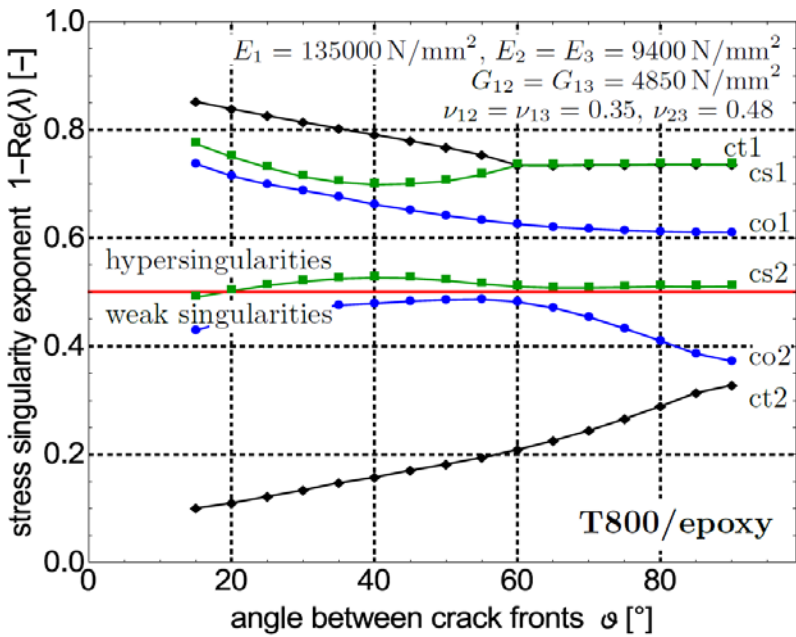


Figure 3: Stress singularity exponents for a delamination crack meeting a transverse inter-fiber crack in a T800/epoxy CFRP laminate with ply-layups [(90°-9)/90°].

The classical crack singularity value, marked by a red line in Figure 3 and Figure 4, separates weak singularities from strong singularities, which we also call hypersingularities. It again emphasized that weak singularities can be classified as less critical than the classical crack singularities, as they yield a differential energy release rate of G = 0 and, therefore, favor a crack arrest. On the other hand, hypersingularities yield a differential energy release rate of $\mathcal{G} \to \infty$, which obviously favors growth. crack For all crack configurations studied, only two stress singularities are weak, which are the ones associated deformation modes co2 and ct2. In

contrast, always three hypersingularities are present, namely those associated to deformation modes co1, cs1 and ct1. Moreover, it can be stated that strong singularities become even stronger with decreasing angle ϑ while the weak singularities decline or at least remain weak. Please also note that the real part of the stress singularity exponents associated to the deformation modes cs1 and ct1 are the same for angles $\vartheta \gtrsim 60^\circ$. This is because they constitute a pair of complex conjugated stress singularity exponents which makes them occur strongly interconnected (cf. eq. (15)). However, all other stress singularities found for the considered T800/epoxy laminate configurations are not complex.

For comparison, configurations with less anisotropic ply materials were studied: a delamination meeting a transverse inter-fiber crack in a typical $[(90^{\circ} - 9)/90^{\circ}]$ glass fiber reinforced plastics (GFRP) laminate and the same geometrical setup but in a homogeneous isotropic body (Figure 4). The material data are given in the figures while the stress singularities present in a homogeneous isotropic body only depend on Poisson's ratio but not on Young's modulus. Here again, all

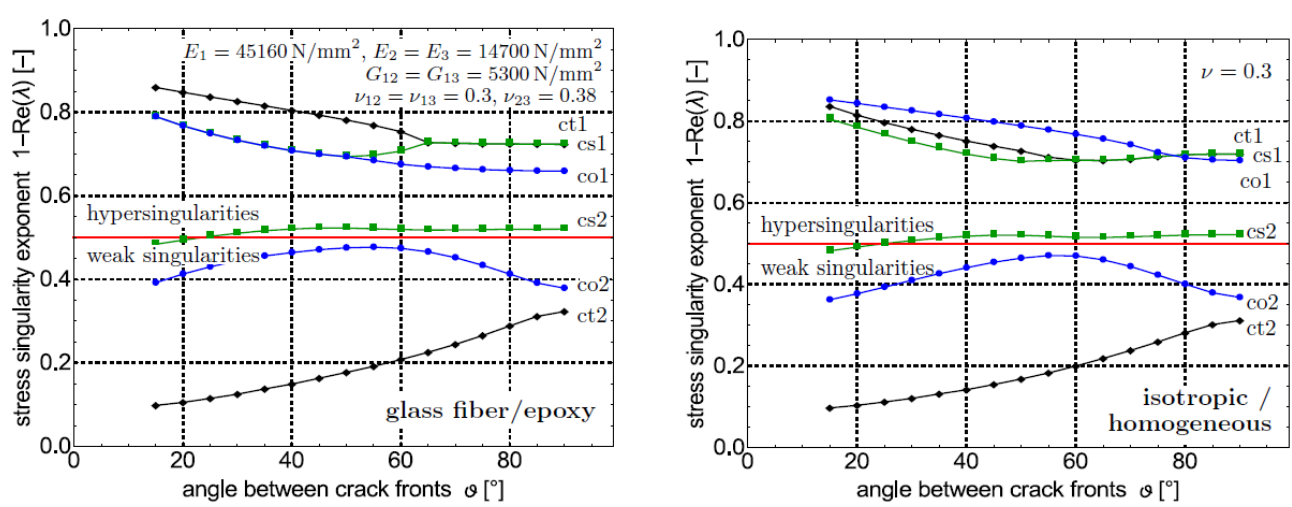


Figure 4: Stress singularity exponents for two meeting cracks with perpendicular mode I crack growth directions in a (a) typical GFRP laminate with ply-layups [(90°-9)/90°] and a (b) homogeneous isotropic body.

configurations considered go along with 3 hypersingularities, 2 weak singularities and one singularity approximately matching the classical crack singularity. From Figure 3 and Figure 4 it can be seen that the material properties mainly affect deformation mode co1. Its dependence on the elastic contrast between the upper and the lower ply is expected as it also plays a major role for the stress singularity exponent of the crack opening mode of a single crack impinging an interface (e.g. [Bogy (1971); Ting and Hoang (1984)]). The other deformation modes seem to be hardly or only moderately affected by the material properties. Finally, complex singularities can also be found for GFRP laminates and homogeneous isotropic materials. The considered GFRP laminate exhibits complex singularities for angles between the crack fronts of $50^{\circ} \gtrsim 9 \gtrsim 65^{\circ}$ and the homogeneous isotropic configuration with a Poisson's ratio of $\nu = 0.3$ for angles $9 \gtrsim 60^{\circ}$. Although the magnitude of the imaginary part of the stress singularity exponent is always rather small with $|\text{Im}(\lambda)-1| < 0.045$, it is remarkable that, here, a complex singularity can also occur in the homogeneous isotropic case.

Conclusion

The SBFEM has been used to solve boundary value problems of linear elasticity which contain singular points. Even 3D anisotropic structural situations involving interfaces are treated accurately and efficiently. Such a structural situation is the one of a delamination crack meeting a transverse inter-fiber crack, which has been treated in this contribution. It has been shown that this is a highly critical structural situation involving up to 3 hypersingularities. This strongly motivates a further investigation. It is worth pointing out that the hypersingularities found can be complex singularities - even in the simplified homogeneous isotropic case of this geometrical setup.

Acknowledgment

The authors highly appreciate the financial support of the German Research Foundation (DFG), project BE1090/35-1.

References

- Bažant, Z.P. and Estenssoro, L.F. (1979) Surface singularity and crack propagation, *International Journal of Solids and Structures* **15**, 405-426.
- Behnke, R., Mundil, M., Birk, C. and Kaliske, M. (2014) A physically and geometrically nonlinear scaled-boundary-based finite element formulation for fracture in elastomers. *International Journal for Numerical Methods in Engineering* **99**. 966-999.
- Bogy, D.B. (1971) On the plane elastostatic problem of a loaded crack terminating at a material interface. *Journal of Applied Mechanics* **38**, 911-918.
- Deeks, A.J. and Wolf, J. P. (2002) A virtual work derivation of the scaled boundary finite-element method for elastostatics. *Computational Mechanics* **28**, 489-504.
- Dimitrov, A., Andrä, H. and Schnack. E.(2001) Efficient computation of order and mode of corner singularities in 3d-elasticity. *International Journal for Numerical Methods in Engineering* **52**, 805-827.
- Ghahremani, F. (1991) A numerical variational method for extracting 3D singularities. *International Journal of Solids and Structures* **27**, 1371-1386.
- Goswami, S. and Becker, W. (2012) Computation of 3-d stress singularities for multiple cracks and crack intersections by the scaled boundary finite element method. *International Journal of Fracture* **175**, 13-25.
- Hell, S. and Becker, W. (2014) Hypersingularities in three-dimensional crack configurations in composite laminates. *Proceedings in Applied Mathematics and Mechanics* **14**, 157-158.
- Koguchi, H. and da Costa, J.A. (2010) Analysis of the stress singularity field at a vertex in 3D-bonded structures having a slanted side surface. *International Journal of Solids and Structures* **47**, 3131-3140.
- Korepanova, T.O., Matveenko, V.P. and Sevodina, N.V. (2013) Numerical analysis of stress singularity at singular points of three-dimensional elastic bodies. *Acta Mechanica* **224**, 2045-2063.
- Leguillon, D. and Sanchez-Palencia, E. (1999) On 3d cracks intersecting a free surface in laminated composites. *International Journal of Fracture* **99**, 25-40.

- Leguillon, D. and Martin, E. (2012) Crack nucleation at stress concentration points in composite materials Application to the crack deflection by an interface. *Mathematical Methods and Models in Composites, Computational and Experimental Methods in Structures* **5**, 401-424.
- Leguillon, D. and Martin, E. (2013) The strengthening effect caused by an elastic contrast part i: the bimaterial case. *International Journal of Fracture* **179**, 157-167.
- Mittelstedt, C. and Becker, W. (2005) Semi-analytical computation of 3d stress singularities in linear elasticity. *Communications in Numerical Methods in Engineering* **21**, 247-257.
- Mittelstedt, C. and Becker, W. (2006) Efficient computation of order and mode of three-dimensional stress singularities in linear elasticity by the boundary finite element method. *International Journal of Solids and Structures* **43**, 2868-2903.
- Ooi, E.T., Song, C. and Tin-Loi, F. (2014) A scaled boundary polygon formulation for elasto-plastic analyses. *Computer Methods in Applied Mechanics and Engineering* **268**, 905-937.
- Somaratna, N. and Ting, T.C.T. (1986) Three-dimensional stress singularities in anisotropic materials and composites. *International Journal of Engineering Science* **24**, 1115 -1134.
- Song, C. (2006) Analysis of singular stress fields at multi-material corners under thermal loading. *International Journal for Numerical Methods in Engineering* **65**, 620-652.
- Song, C. and Wolf, J.P. (1997) The scaled boundary finite-element method alias consistent infinitesimal finite-element cell method for elastodynamics. *Computer Methods in Applied Mechanics and Engineering* **147**, 329-355.
- Ting, T.C.T. and Hoang. P.H. (1984) Singularities at the tip of a crack normal to the interface of an anisotropic layered composite. *International Journal of Solids and Structures* **20**, 439-454.
- Wolf, J. P. (2003) The scaled boundary finite element method. John Wiley & Sons, Chichester, UK.